Hindawi Publishing Corporation
International Journal of Antennas and Propagation
Volume 2015, Article ID 245621, 15 pages
http://dx.doi.org/10.1155/2015/245621

Research Article

An Efficient Full-Wave Electromagnetic Analysis for Capacitive Body-Coupled Communication

Muhammad Irfan Kazim,[1] Muhammad Imran Kazim,[2] and J. Jacob Wikner[1]

[1]*Department of Electrical Engineering, Linköping University, 581 83 Linköping, Sweden*
[2]*Department of Electrical Engineering, Eindhoven University of Technology (TU/e), P.O. Box 513, 5600 MB Eindhoven, Netherlands*

Correspondence should be addressed to Muhammad Irfan Kazim; irfan.kazim@isy.liu.se

Received 16 February 2015; Revised 28 April 2015; Accepted 4 May 2015

Academic Editor: Lorenzo Crocco

Measured propagation loss for capacitive body-coupled communication (BCC) channel (1 MHz to 60 MHz) is limitedly available in the literature for distances longer than 50 cm. This is either because of experimental complexity to isolate the earth-ground or design complexity in realizing a reliable communication link to assess the performance limitations of capacitive BCC channel. Therefore, an alternate efficient full-wave electromagnetic (EM) simulation approach is presented to realistically analyze capacitive BCC, that is, the interaction of capacitive coupler, the human body, and the environment all together. The presented simulation approach is first evaluated for numerical/human body variation uncertainties and then validated with measurement results from literature, followed by the analysis of capacitive BCC channel for twenty different scenarios. The simulation results show that the vertical coupler configuration is less susceptible to physiological variations of underlying tissues compared to the horizontal coupler configuration. The propagation loss is less for arm positions when they are not touching the torso region irrespective of the communication distance. The propagation loss has also been explained for complex scenarios formed by the ground-plane and the material structures (metals or dielectrics) with the human body. The estimated propagation loss has been used to investigate the link-budget requirement for designing capacitive BCC system in CMOS sub-micron technologies.

1. Introduction

Capacitive body-coupled communication (BCC) is considered an enabling short-range wireless technology for the interaction between humans and the smarter ambiance. The useful frequency range falls between hundreds of kHz to tens of MHz [1]. The capacitive BCC has an advantage over other wireless technologies like Bluetooth and Zig-bee in the context of personal area network (PAN) and internet-of-things (IOT) due to lower power consumption and confinement of radiated energy, thus requiring less allocation of special frequency bands for communication. However, the potential of capacitive BCC for the aforesaid applications could be fully utilized by understanding the realistic interaction of the capacitive coupler, the human body (electrophysiological properties of tissues), and the environment for different scenarios and communication distances. Although different chip solutions have been presented for capacitive BCC [2, 3], it is not clearly known for how many body positions and for which coupler configuration/sizes, communication distances, environment, and so forth the results have been reported. A limited literature about experimental measurements for the propagation characteristics of capacitive BCC channel is available, the limitation being the experimental setup, especially for distances longer than 50 cm. A number of factors which influence BCC include large variations in the propagation characteristics with different body positions, coupler types and sizes, types of indoor flooring, furniture, and electronic equipment around us. The other factors encompass the difficulties in isolating the earth-grounded instruments during body measurements and design complexity involved in implementing reliable, battery-operated, high data-rate transceivers in the mid-frequency range of 1 MHz to 60 MHz for bit-error-rate (BER) measurements.

An alternate approach is to rely on circuit based models [4, 5] or analytical [6] or numerical methods [7–11] to model

and analyze the capacitive BCC channel. This paper proposes a systematic efficient full-wave electromagnetic (EM) approach to analyze capacitive BCC channel propagation loss characteristics and the influence of the aforesaid factors. The analysis, after validation with the measurement results, considers the combined interaction of the capacitive coupler of different types and sizes, the human body (electrophysiological properties of tissues), and the environment to explain propagation loss for complex scenarios. Moreover, different body positions have also been analyzed over the useful frequency range of 1 MHz to 60 MHz for communication distances longer than 50 cm.

This paper is divided into five sections. Section 2 presents an overview and comparison of the literature about the modeling of capacitive BCC channel. Section 3 describes the proposed efficient full-wave EM approach for analyzing capacitive BCC. The evaluation for numerical/human body variation uncertainties and validation with the measurement results from the literature of the proposed approach is also presented in this section. The effects of coupler configurations, human body, and the environment are estimated from the propagation loss curves and the electric field intensity plots, which defines the scope of Section 4. The investigation of link-budget requirement based on the estimated propagation loss is also carried out in this section, followed by the concluding remarks in Section 5.

2. Literature Review: Modeling of Capacitive BCC Channel

Different propagation models for capacitive BCC channel have been proposed in the literature with confined applicable scope. Zimmerman [4], who pioneered this field, presented an electrical model which is based on electrostatic coupling between transmitter (Tx) and receiver (Rx) capacitive electrodes and their capacitive return path through external ground, considering the human body as a perfect electric conductor (PEC) with zero impedance. This lumped capacitive model has been extended to a distributed parallel RC equivalent circuit model [5]. The values of resistance (R) and capacitance (C) in this model have been derived from the equivalent homogeneous human phantom model of muscle for arm-torso-arm region, considering conduction current and voltage drop inside human body. The limitation with Zimmerman model [4] is that it perhaps takes into account one particular scenario for empirically calculating the body and electrode capacitance from measured path impedance (possibly, some typical values were also used in the model whose adapted strategy for estimation is not clearly known). Similarly distributed RC parallel circuit values in [5] have been empirically calculated from the considered homogeneous phantom model (σ = 0.2 S/m & ϵ_r = 70) for one particular scenario. Moreover the earth-grounded instruments used in [5] also raises questions on the applicability of these derived circuit parameters for practical scenarios. The lumped coupling capacitance values suggested in the Zimmerman model were estimated numerically in [7–9]. Reference [7] proposed a four-terminal equivalent circuit model with six impedances for two- and four-electrode arrangements. The capacitance was determined numerically under the electrostatic assumption using finite element method (FEM). The transmission gain calculated by this circuit model was compared with the measured results at 1 kHz, 10 kHz, 100 kHz, and 1000 kHz but the instruments used in the measurement were not battery-operated but rather earth-grounded, thereby indirectly sharing the common ground. Another equivalent circuit model presented in [8] numerically calculated the mutual capacitance for different scenarios by the method-of-moments (MoM) which were also verified by finite-difference time-domain (FDTD) method. The different scenarios include no-conductor grounded, body grounded, and transmitter or receiver grounded under quasi-electrostatic assumption, considering human body as a perfect electrically conducting sphere with negligible induced currents. This model was refined in [9] by proposing an equivalent circuit model based on lossy conductors inducing conduction currents inside the human arm phantom. The capacitance values were estimated by the numerical analysis technique of MoM and verified by FDTD. The relative permittivity and conductivity of the human arm phantom used in [9] correspond to that of human muscle tissue only. The capacitance due to the outer most skin and fat dielectric layers have not been taken into consideration (while evaluating the equivalent lumped capacitance). The conductivity of muscle tissue is higher than outermost skin and fat tissues which undermines the proposed model. Reference [6] has considered the surface of human body as an infinite half-plane with skin-only tissue properties for vertical electric-dipole type coupler. The analytical model [6] uses the derivation in [12, 13] for defining the vertical component of the electric field intensity due to the vertical dipole. The electric field intensity expression after simplification includes the surface wave far-field propagation with attenuation factor, reactive inductive field radiation, and quasi-static near-field terms. This model takes into account the electrophysiological properties in terms of relative permittivity and conductivity of the human skin which is explicitly included in the expression of surface wave attenuation factor. But on the other hand, this model generalizes the finite-sized vertical coupler configuration with a theoretical infinitesimal dipole which results in deviation between theoretical and measured results and is more pronounced when the coupler dimensions and communication distances are comparable. Reference [10] considered the electrophysiological properties of skin and underneath living tissues in 3D finite element model of human upper arm under quasi-electrostatic conditions to study the attenuation characteristics but their study was limited to 1 MHz. The dielectric values used in this simulation model from [14] have larger uncertainties than average for frequencies below 1 MHz. Moreover the effects of external environment and earth-ground on the signal or propagation loss have also not been presented. Reference [11] considered the combined effect of coupler, muscle equivalent human body model, and environment (earth-ground and material structures) at 10 MHz but the simulation results are limited to fixed size coupler, fixed distance (19 cm) between couplers, and same body position.

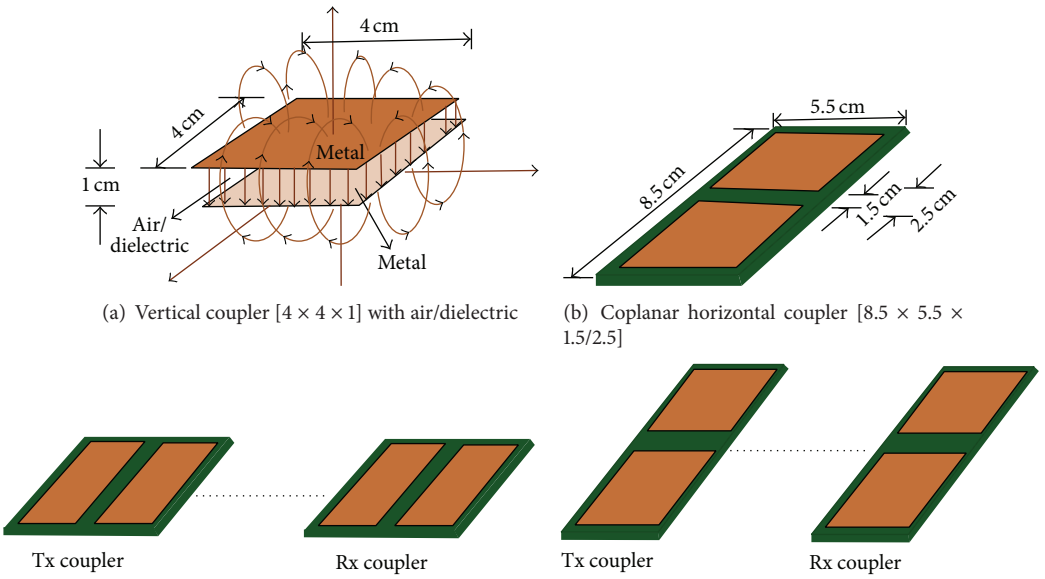

(a) Vertical coupler [4 × 4 × 1] with air/dielectric

(b) Coplanar horizontal coupler [8.5 × 5.5 × 1.5/2.5]

(c) Coplanar horizontal coupler (Longitudinal orientation)

(d) Coplanar horizontal coupler (Transversal orientation)

Figure 1: Coupler configurations and their orientations.

A summary of the reviewed literature concerning the modeling of capacitive BCC channel is summarized in Table 1 with pros and cons. The figures-of-merit for the comparison are based on the realistic modeling of the interaction of the variable coupler sizes/types, the human tissues physiological properties, and the environment all together for different body positions over the useful frequency range of 1 MHz to 60 MHz, communication distances longer than 50 cm, provision of propagation model cosimulation in circuit simulator, and computational efficiency. As can be seen from Table 1, the approaches presented in the reviewed literature have limitations in analyzing the interrelated effects of different parameters. The challenge is to model the problem as close to the real setup as possible, without making it computatively too intensive to handle. The presented approach in this paper is based on efficient full-wave EM solution to realistically model and understand the capacitive BCC with the provision of creating different scenarios over the useful frequency/communication distance range. Although full-wave EM solution is computatively intensive in comparison to the equivalent circuit model and analytical approaches, the presented approach reduces the complexity of the problem with the simplified assumptions while quantifying the tolerance bounds.

3. Efficient Full-Wave EM Approach

An efficient full-wave EM approach for realistic modeling of capacitive BCC channel is presented in this section. For the capacitive BCC modeling, the interaction of the coupler, the whole human body (considering electrophysiological properties of tissues), and the environment all together is of importance. The modeling of the human body is very complex and is the main contributing factor towards increasing the computational cost of any analysis. The presented approach carries out the modeling of human body by analyzing the effects of stratification and curvature. A single tissue layer of the whole human model with quantifiable tolerance bounds is considered afterwards for analysis to make the approach computatively efficient. The full-wave EM approach makes use of the 3D EM tool of Computer Simulation Technology (CST) Microwave Studio (MWS) for modeling of the capacitive BCC channel. CST is a 3D electromagnetic simulator based on Finite Integration Technique (FIT) [18], which "*provides discrete reformulation of Maxwell's equations in their integral form*" [19]. The Maxwell equations are numerically solved over the finite calculation domain enclosing the considered problem. A suitable mesh splits this domain into many small grid cells for which the equations are solved separately.

The following section first highlights the coupler configurations and the environment, followed by the efficient human body modeling by incorporating simplified assumptions. The above is discussed both in general and in context with CST MWS software. The efficient full-wave EM approach is evaluated for numerical/human body variation uncertainties and validated afterwards with the measurement results of the literature.

3.1. Coupler Configurations and Environment. The front-end of the transmitter or receiver for capacitive BCC channel consists of an electrode coupler structure which is capacitive in nature. The configurations of the coupler (vertical/horizontal) with different orientations (longitudinal/transversal) are shown in Figure 1. The normally used vertical couplers comprise two metal layers with air or dielectric material in between. The two metal structures in

Table 1: Summary and comparison of the reviewed literature concerning the modeling of capacitive BCC channel.

Literature review [reference]	BCC propagation model	Coverage of modeling aspects			Model covering different scenarios			Cosimulation model/circuit provision	Computational efficiency
		Coupler sizes/types	Body tissues physiology	Environment	Body positions	Frequency (1 to 60 MHz)	Tx/Rx distance ≥50 cm		
[4, 5]	Equivalent circuit	Fixed size [4], no [5]/no	No [4], phantom [5]	No	No	No [4], 10 to 60 MHz [5]	No [4], yes [5]	Yes	Yes
[7–9]	RC estimate MOM/FDTD	No/yes [7], no	No, muscle equivalent [9]	No	No	No	No	Yes	Partial
[6]	Analytical (*curve-fitting*)	Infinitesimal dipole/no	Skin-only	No	No	Yes	Yes	No	Yes
[10]	FEM quasi-electrostatic	Fixed size/no	Skin-only	No	Yes	No	No	Not mentioned	Partial
[11]	FDTD	Fixed size/no	Muscle equivalent	Yes	No	No	No	Not mentioned	Partial
This work	Efficient full-wave EM	Variable size/yes	Stratified & skin-only	Yes	Yes	Yes	Yes	Yes (*S*-matrix)	Partial*

*Full-wave EM is a numerical technique, computatively intensive; however, an approach of making it efficient yet accurate is presented.

horizontal configuration are separated by some distance on the same side of the substrate. The horizontal and vertical coupler dimensions are expressed in this paper as [length × breadth × horizontal/vertical spacing] described in Figure 1.

External objects (aluminium/wood table, steel cupboard) and different types of flooring (earth-ground) need to be considered for capacitive BCC channel modeling. In CST MWS, the external objects can be modeled using different conductive and dielectric materials, whereas the electric boundary condition can be used to simulate the earth-ground flooring.

3.2. Human Body Modeling. The human body comprises a number of layers, each having its own dielectric properties which are frequency dependent. The dispersion properties, in terms of complex permittivity (ϵ' [real] and ϵ'' [imaginary]), for the four considered layers are determined from the effective conductivity (σ_e) and the relative permittivity (ϵ_r) values [15] and the use of the following relationships:

$$\begin{aligned} \epsilon' &= \epsilon_0 \epsilon_r, \\ \epsilon'' &= \epsilon' \tan\delta, \\ \tan\delta &= \frac{\sigma_e}{2\pi f \epsilon'}, \end{aligned} \tag{1}$$

where tanδ is the loss-tangent of the dielectric and f is the frequency. In CST MWS, the dispersion properties of each layer can be specified by using the dispersion list in the material properties. The dispersion list takes the normalized values of ϵ' and ϵ'' with respect to the free-space permittivity ϵ_0. The normalized values of complex permittivity (ϵ' [real] and ϵ'' [imaginary]) of dry skin, fat, muscle, and bone cortical from 1 MHz to 60 MHz, which has been used in four-layer-stratified and skin-only models in CST MWS, have been plotted in Figure 2. These values are based on the parametric model of four Cole-Cole type dispersion and parameter values presented in [14, 15]. This model is reliable for frequencies above 1 MHz [14] which is also the reason for selecting 1 MHz as the lower frequency for capacitive BCC channel in this work. The human arm models have been considered first to study the effect of stratification and curvature. Figure 3(a) represents the standard four-layer-stratified (Str4) model of a human arm [20] used in this work, starting from the outermost layer of skin to the innermost bone medium.

3.3. Simulation Setup. The transient solver of CST MWS has been used to study the effect of the stratification and curvature of human model (Figures 3(a)–3(d)) on the BCC. The transient solver allows simulation of the model behavior over a wide frequency range in a single computation run, resulting in efficient computation for problems with open boundaries and large dimensions. The accuracy of the field solution increases with a finer mesh at the cost of increased computation time. Therefore, both the global and local mesh refinement techniques have been used. The open boundary conditions have been defined to study the variation in

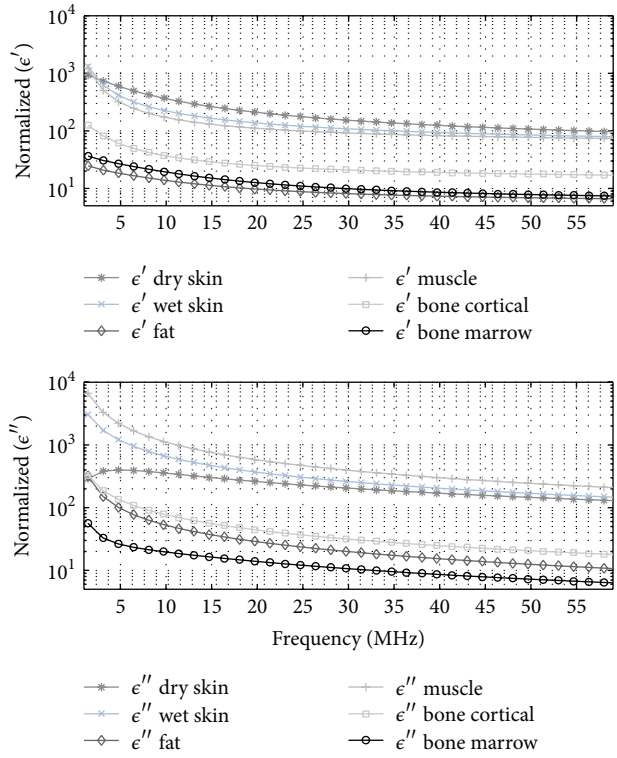

Figure 2: Normalized complex permittivity, that is, normalized ϵ' (real) and normalized ϵ'' (imaginary) values of dry skin, fat, muscle, and bone cortical from 1 MHz to 60 MHz [15], used in four-layer-stratified model in CST MWS.

propagation losses for the three cases (skin-only-cylinder (Sk-Cyl), skin-only-rectangle (Sk-Rec), and standard four-layer-stratified (Str4)) with variation of distance (d) to 20 cm, 40 cm, and 90 cm for a pair of two different coupler structures (vertical [6 × 6 × 3] and horizontal [5 × 2 × 1]) on transmitter and receiver sides. For the excitation of the coupler, CST has the provision of using either the wave guide or the discrete port. The selection of the specific port depends on the ease-of-use for problem under investigation. For the inhomogeneous model like four-layer human arm model, the discrete port is the preferred choice to avoid instability issues faced with wave guide port. The discrete ports of 50 ohms have been used to compare the arm models shown in Figures 3(b), 3(c), and 3(d) to observe the relative variation of the propagation loss for the three cases. The four-layer-stratified model is closer to real human but it required around 1 million mesh cells which were reduced by almost 5 times for the skin-only-cylinder and rectangle models. The simulation time was also reduced by a factor of 10 for the skin-only models. The propagation loss (L) is determined from the scattering (S) parameter S_{21} as

$$L\,(\text{dB}) = 20\log_{10}\frac{1}{|S_{21}|}, \tag{2}$$

where port 1 and port 2 are signifying transmission and reception sides, respectively. For symmetrical capacitive BCC scenarios, $|S_{12}| = |S_{21}|$.

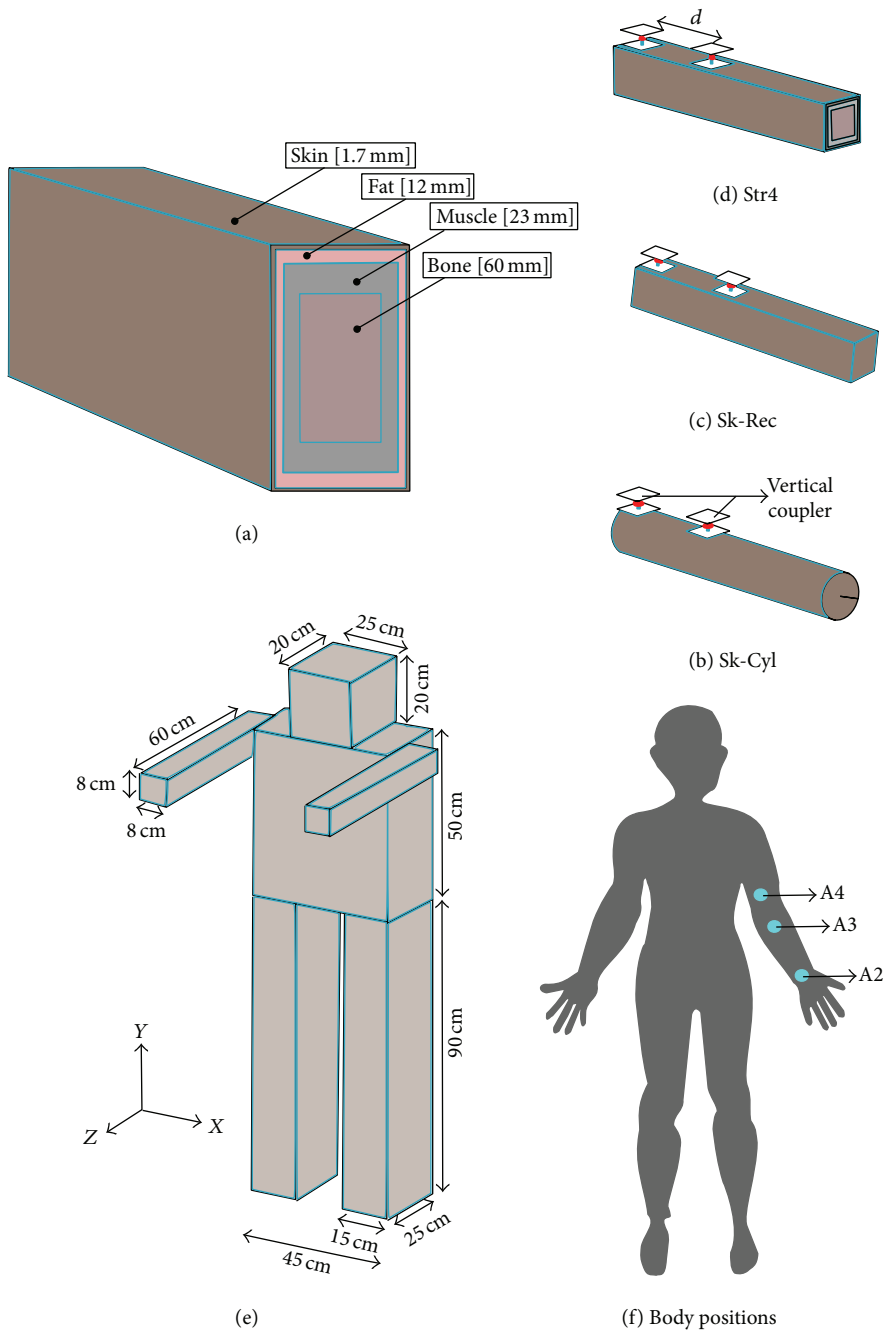

Figure 3: Comparison of different models with couplers (shown for vertical electrodes only). (a) Cross-sectional view of the standard four-layer-stratified (Str4) human arm model (layer thickness is shown in square brackets), (b) skin-only-cylinder (Sk-Cyl) model, (c) skin-only-rectangle (Sk-Rec) model, (d) standard four-layer-stratified (Str4) model, (e) the skin-only-rectangle human body model with all the dimensions, and (f) body positions for validation with the measurements from literature.

3.4. Evaluation for Numerical/Human Body Variation Uncertainties. The proposed efficient full-wave EM simulation approach has been evaluated by taking the effects of numeric uncertainties (boundary conditions, mesh cells) and human body variation uncertainties (dielectric properties, dielectric thicknesses) independently. The systematic variations of simulation parameters have been performed for Str4 human arm model (shown in Figure 4) and skin-only-rectangle human body model (shown in Figure 6) for both the vertical and horizontal couplers.

3.4.1. Numerical Uncertainties

Boundary Conditions. The added spacing of open added space (OAS) boundary condition (BC) is varied between 1/8th and 1/2nd of wavelength (at the center frequency of 30 MHz) in

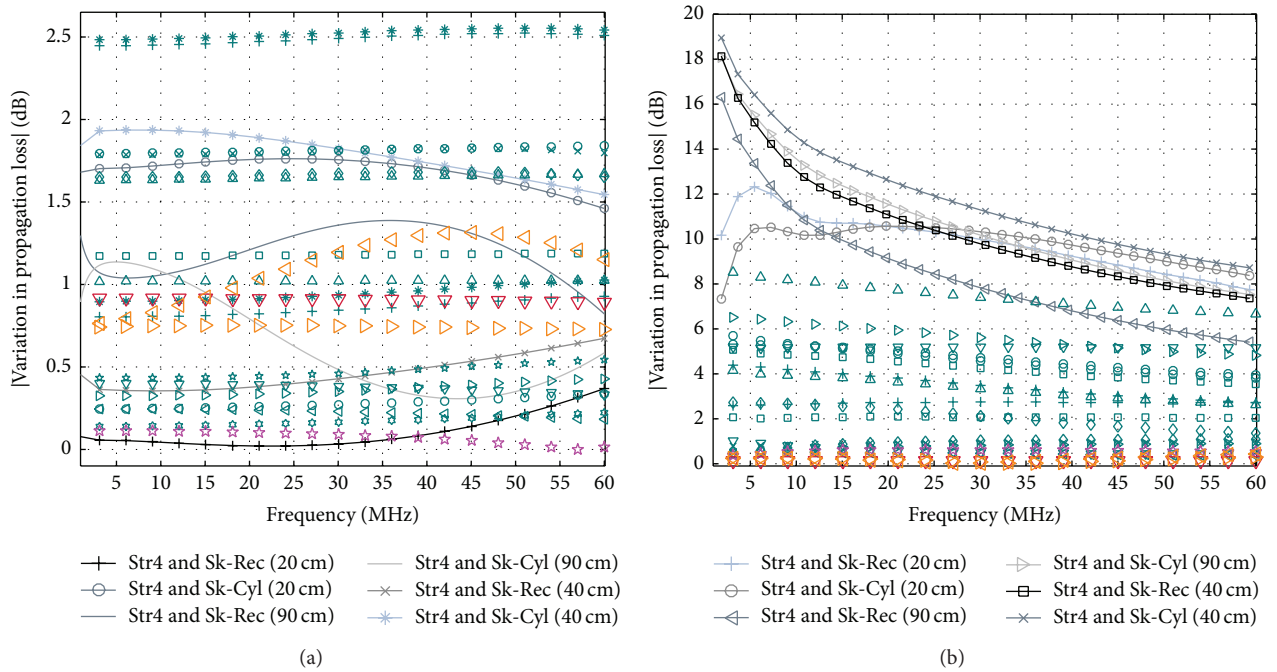

FIGURE 4: Variation in propagation loss among three human arm models: skin-only-cylinder (Sk-Cyl), skin-only-rectangle (Sk-Rec), and standard four-layer-stratified (Str4) for distances 20 cm, 40 cm, and 90 cm with (a) vertical couplers [6 × 6 × 3], (b) horizontal couplers [5 × 2 × 1]; all coloured symbols show variations with boundary conditions, mesh sizes, dielectric properties, and dielectric layer thicknesses for Str4 human arm model with 40 cm distance.

X, Y, and Z directions for the human arm model. For the human body model, in addendum to the above, open BC on Y-min (bottom) with OAS in all other directions have been considered, denoted as E-OAS.

Mesh Cells. The increase in mesh cells (3-4 times) from the recommended setting (at least 2-3 mesh lines for the smallest region) has been considered.

3.4.2. Human Body Variation Uncertainties

Dielectric Properties. The variation of ±12% is taken for all the layers of Str4 human arm model and skin layer of human body model.

Dielectric Thickness. Almost ±17% variation is considered for different combinations of skin, fat, muscle, and bone of Str4 human arm model with no thickness variation for human body model.

Figures 4(a) and 4(b) show the relative difference in propagation loss variations between Str4 and Sk-Cyl/Sk-Rec for vertical and horizontal coupler configurations, respectively. The effect of systematic variations (boundary conditions, mesh cells, dielectric properties, and dielectric layer thicknesses) for Str4 human arm model with 40 cm distance is also shown. The dark orange triangle, teal, red, and magenta coloured symbols show the effect of the considered variation of dielectric properties, dielectric thickness, boundary conditions, and mesh cells, respectively. It can also be observed from the transient solver simulation results shown in Figure 4(a) that the relative difference in propagation loss variations between standard four-layer-stratified (Str4) and skin-only-rectangle (Sk-Rec) and skin-only-cylinder (Sk-Cyl) is very small (within 2.5 dB) for vertical coupler configuration over 20 cm, 40 cm, and 90 cm distances from 1 MHz to 60 MHz. However for the horizontal coupler configuration, the difference is comparatively larger (between 10 dB to 20 dB) for frequencies between 1 MHz and 15 MHz but reduces for frequencies higher than 15 MHz, as shown in Figure 4(b). This comparison reveals that the skin-only-rectangle arm model is sufficiently accurate for vertical coupler configuration and can be used for simplification purposes. However, the propagation characteristics due to the horizontal coplanar couplers are dependent to a larger extent on the dispersive properties of the underlying tissue layers in the human body model. It is worth mentioning here that the valuable computation time is reduced due to the lesser number of mesh cells' requirement in CST MWS for the skin-only models in comparison with standard four-layer-stratified model as mentioned earlier. Moreover, it can also be seen that the effect of curvature for skin-only-cylinder model does not result in significant variation of the propagation loss compared to skin-only-rectangle model for both vertical (2 dB) and horizontal (3 dB) coupler configurations. The simulations have been performed for skin-only-rectangle human body model as well by varying number of mesh cells, boundary conditions, and skin dielectric properties for *arm position f* (135 cm distance) of Figure 7(b) for both vertical and horizontal coupler configurations. The simulation results in Figure 6 show that the error bounds are within the acceptable limits for skin-only-rectangle human body model.

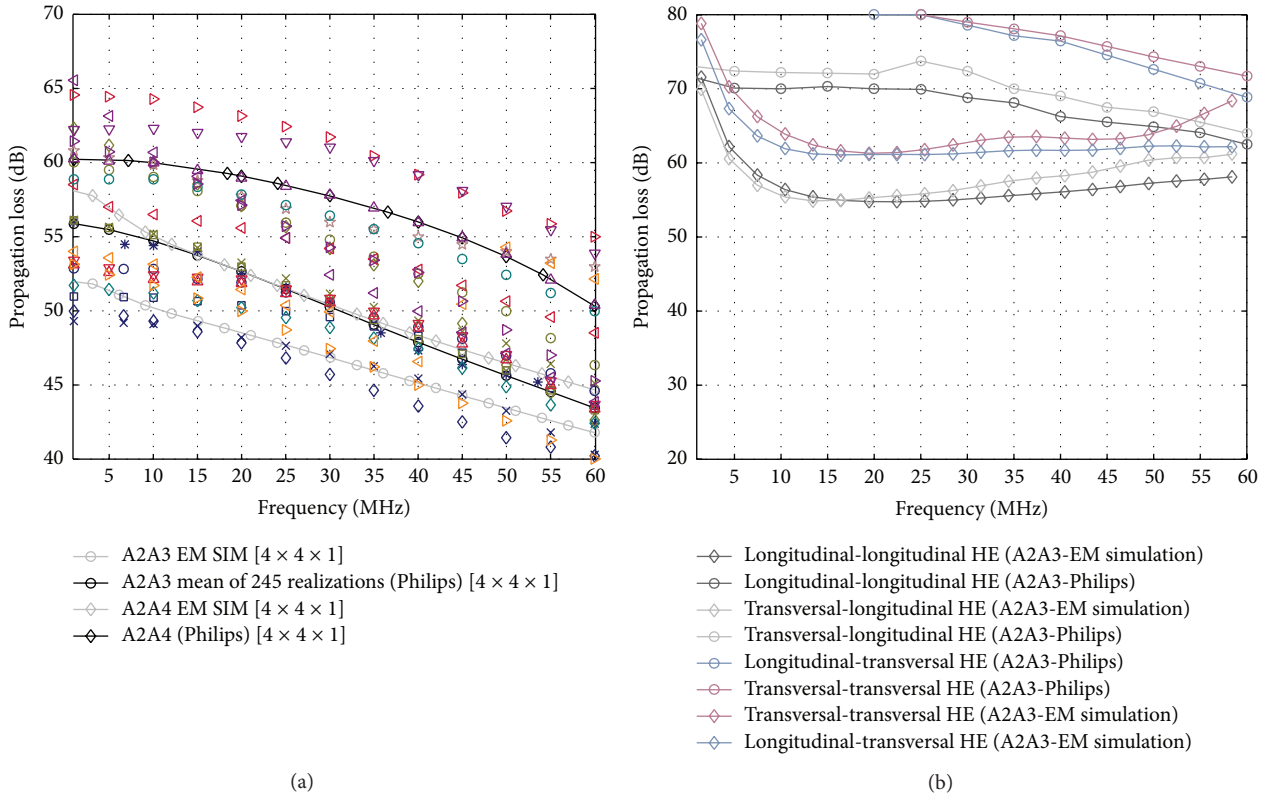

Figure 5: 3D full-wave EM simulation results compared with Philips measurement results [1, 16, 17] for the skin-only-rectangle (Sk-Rec) human body model with (a) vertical couplers [4 × 4 × 1] for A2A3 and A2A4 path lengths (the coloured symbols show variations in Philips measurements with respect to coupler dimensions, separation, construction, and body position/movements), (b) horizontal couplers [5 × 2 × 1] having different orientations for A2A3 path length.

3.5. Validation with the Measurement Results. It is important to validate the proposed efficient EM approach based on the skin-only-rectangle human body model with the measurement results on the actual human body. The simulation results of the last subsection also provide the bounds for the simplified efficient approach for both the vertical and horizontal couplers. Most reported measurement results in the literature do not represent the real propagation loss of the human body. This is either due to the usage of earth-grounded lab instruments or the first-order RC pole like response due to analog front-end limitation which masks the actual human body propagation loss, for example, [5, 7, 21, 22]. The use of baluns also does not help in completely isolating the earth grounds as the parasitic capacitance between primary and secondary windings causes the coupling of common-mode signal [23]. It has been shown in [23] that the maximum difference in the transmission level magnitude measurements is as high as 40 dB for four different types of baluns. Some of the examples from the literature which fall under this category of experimental measurement uncertainty are in [24, 25]. The measurements performed on simplified homogeneous biological human phantoms are not equivalent to real measurements on human body. The examples of experimental measurement uncertainty for human equivalent phantoms from literature are [26] (muscle equivalent phantom at 10 MHz) and [27] (muscle simulating liquid). However, the measured results by Philips research group presented in [1, 16, 17] take care of the above-mentioned experimental setup uncertainties. That is why for validation purposes, the estimated propagation loss from the full-wave EM approach for skin-only-rectangle human body model is compared with the measurement results of Philips research group for both the horizontal and vertical coupling schemes.

The geometrical dimensions of the skin-only-rectangle human body model are shown in Figure 3(e) and the dimensions for horizontal and vertical coupler schemes are taken as reported by Philips [1, 16, 17]. The simulation setup for the validation is the same as mentioned in Section 3.3. For excitation, the wave guide ports have been used as the skin-only model is homogeneous. Since the problem with the inclusion of the whole human body becomes computatively large, local mesh refinements have also been used to reduce the mesh cell requirements. The results are simulated for the two vertical coupler structures on the arm of skin-only-rectangle human body model for different separation distances of A2A3 and A2A4. The distances for A2A3 and A2A4 positions are taken as 16 cm and 26 cm, respectively. The simulated A2A3 propagation loss is compared to the mean of 245 realizations of Philips measurement results as shown in Figure 5(a) which gives confidence on the Philips experimental results and our validation process. Although elbow joint has not been modeled in A2A4 but if the

additional loss of 4 dB is considered for the elbow joint [10] (for larger joints, loss is as large as 8 dB) then the deviation between the measured and simulated results is less than 3 dB for A2A4 path length from 1 MHz to 60 MHz for vertical coupler configuration. The deviation in propagation loss between the measured and simulated results for A2A3 path is less than 3 dB. All coloured symbols other than triangle in Figure 5(a) show variations in measured propagation loss for A2A3 path length for vertical coupler configuration as a function of coupler dimensions/separation, coupler construction, arm orientations, body postures, and movements. All coloured triangular symbols show measured propagation loss variations for A2A4 path length. All these variable factors can be incorporated in our proposed efficient full-wave EM model except for body movements.

Similarly horizontal coupler structures with longitudinal and transverse orientations have been simulated on the skin-only-rectangle human body model for A2A3 path length and compared with Philips measurement results as shown in Figure 5(b). The metallized side of the substrate in the horizontal coupler structure touches the human body. The maximum difference between simulated and measured results is around 15 dB to 18 dB for the horizontal coupler as shown in Figure 5(b) for A2A3 path length, which is consistent with the human arm model variations of Figure 4(b). However, the similar trend is followed in terms of propagation loss for different orientations; for example, the longitudinal-longitudinal one has the lowest propagation loss and the transversal-transversal one has the highest above 20 MHz in both the simulations and measurements.

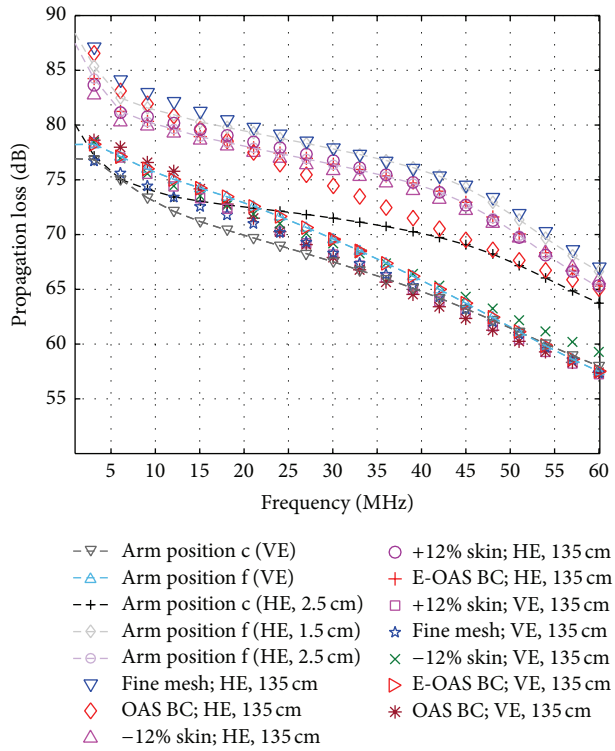

Figure 6: Comparison between horizontal (HE) and vertical (VE) electrode couplers for selected arm positions of Figure 7(b). The effect on propagation loss due to variation of mesh cells, boundary conditions, and skin dielectric properties is shown with coloured symbols for *arm position f* (135 cm distance).

4. Simulation Results for Different Positions/User Scenarios

The validation in the last section for the proposed simplified and efficient full-wave EM approach provides the motivation for further investigating the propagation loss as follows:

(1) Effect of horizontal and vertical couplers.

(2) Effect of body positions, coupler size, and communication distance.

(3) Combined effect of external environment (earth-grounding and material structures).

(4) Effect of ground-plane on resultant electric field.

The above-mentioned effects have been simulated for the propagation loss as discussed below.

4.1. Effect of Horizontal and Vertical Couplers. A comparison of the propagation loss for horizontal and vertical couplers is shown in Figure 6 for selected arm positions of Figure 7(b). The size of horizontal coupler is 5.5 cm × 8.5 cm with 1.5 cm and 2.5 cm horizontal spacing as shown in Figure 1(b). The propagation loss for the vertical coupler of size 4 cm × 4 cm with vertical spacing of 1 cm is at least 10 dB less compared to horizontal couplers for the *arm position f* in Figure 7(b). However, the difference in propagation loss between horizontal and vertical couplers is less for the *arm position c* shown in Figure 7(b). The difference in propagation loss for horizontal couplers with the stratified model is even higher compared to the skin-only-rectangle model shown in Figure 4(b). Therefore, it could be concluded that the vertical couplers have lesser propagation loss than horizontal couplers for the same communication distance and similar sizes of couplers. Another effect is of spacing between the horizontal couplers; the greater the horizontal spacing the lesser the propagation loss. This can be seen in Figure 6 where the propagation loss due to 2.5 cm horizontal spacing is almost 2 dB less than 1.5 cm horizontal spacing for the *arm position f*; the arms stretched outward as shown in Figure 7(b). The smaller horizontal spacing permits higher localized current between the transmitting couplers compared to the receiving couplers [28].

4.2. Effect of Body Position, Coupler Size, and Communication Distance. The effect of different arm positions shown in Figure 7(b) on the propagation loss has been simulated in Figure 7(a) with the vertical coupler configuration. These simulation results are for communication distances longer than 50 cm for which there is limited information available in the literature. The maximum propagation loss is for the *arm position a* shown in Figure 7(b) with diagonal distance of 102 cm between transmitting and receiving couplers. The propagation loss for *arm position f* due to 135 cm distance

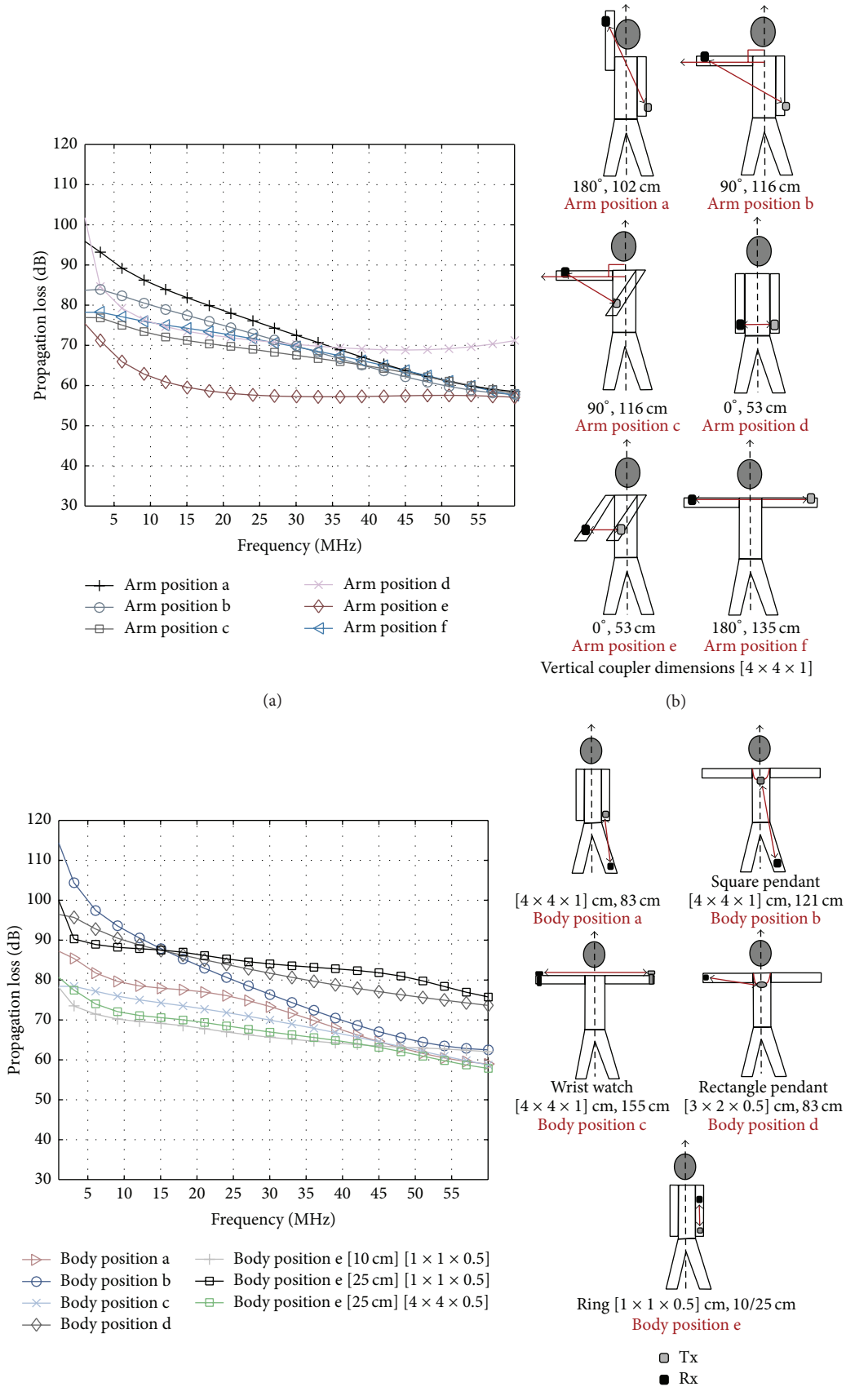

Figure 7: Continued.

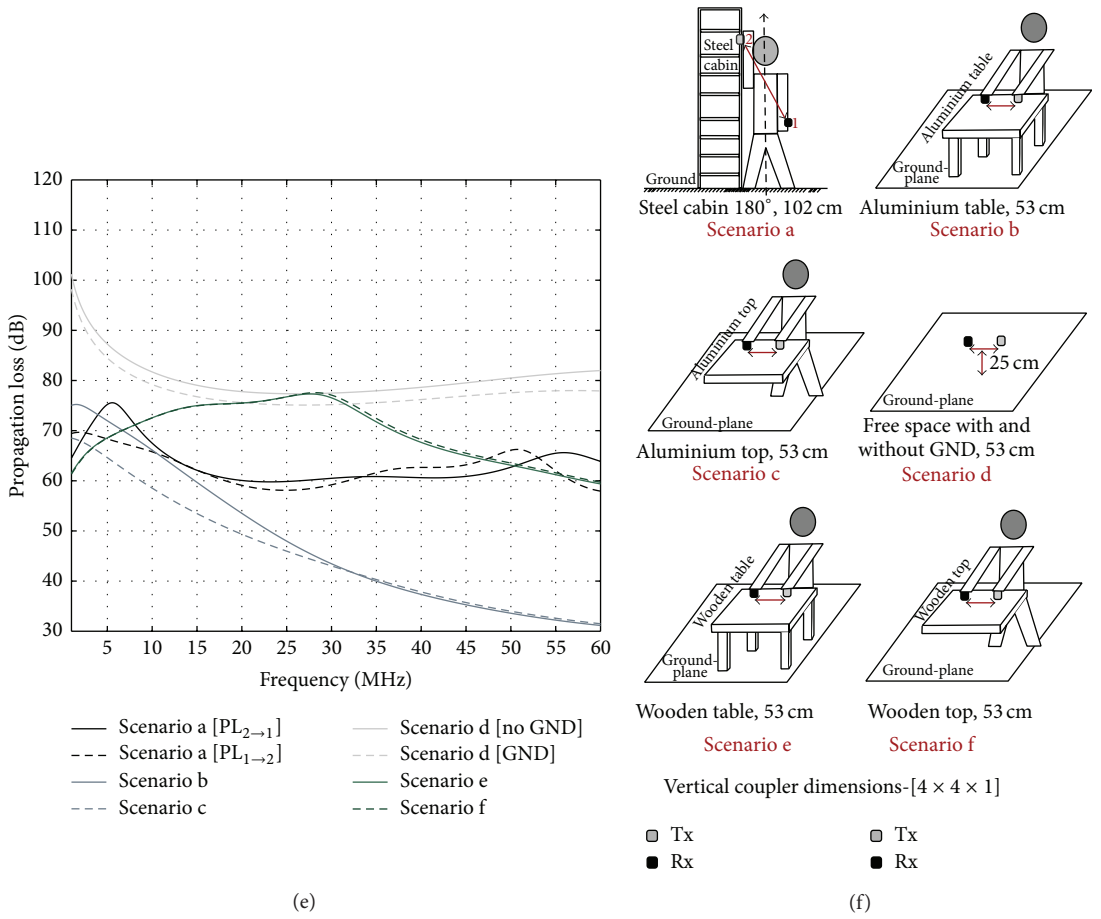

Figure 7: Plots for propagation loss (a), (c), and (e) with vertical coupler configuration for (b), (d), and (f) scenarios, respectively.

is less compared to *arm position a* at lower frequencies; the difference gradually becomes negligible for frequencies more than 40 MHz. Another comparison which emphasizes the importance of body position is between *arm position d* and *arm position e* (53 cm distance) where the difference in propagation loss is approximately 25 dB at 1 MHz and 13 dB to 14 dB over the rest of the frequency range. The better radiation efficiency for frequencies higher than 15 MHz and direct line-of-sight communication together tends to improve the capacitive return path for *arm position d* and *arm position e*. The propagation loss is less up to 30 MHz for *arm position c* compared to *arm position b* for the same distance of 116 cm. The propagation loss for *arm position c* for 116 cm distance is less than the propagation loss for *arm position d* for 53 cm distance. All these simulation results indicate that the propagation loss cannot be just scaled up for the longer communication distance based on the shorter distance, without taking into consideration the specific body positions. It could also be easily deduced that the best positions are when arms are away from the torso region.

Body wearables, for example, wrist watch, pendant, or ring, impose limitations on vertical coupler dimensions whose effect on the propagation loss has been simulated in Figure 7(c) for different body positions in Figure 7(d). The propagation loss due to *body position c* having 155 cm distance is less for *body position a* with 83 cm distance. The propagation loss due to *body position c* (155 cm distance) is also less than *body position b* with 121 cm distance.

Table 2 summarizes comparison of specific coupler/body positions in Figures 7(b) and 7(d) for higher propagation loss. This comparison indicates that it is not only the distance but also the specific body position which matters in determining the propagation loss characteristics and we cannot correctly predict the propagation loss for longer distances based on the measurements of smaller distances as mentioned earlier.

There is a propagation loss of more than 90 dB for frequencies below 10 MHz for rectangle pendant with coupler size of [3 × 2 × 0.5] vertical spacing for *body position d* which makes the receiver design difficult. The requirement of reduced dimensions [1 × 1 × 0.5] for ring configuration results in the increased values of propagation loss compared to [4 × 4 × 0.5] for same distance of 25 cm for *body position e*. The additional propagation loss of approximately 20 dB at the communication distance of 25 cm compared to 10 cm for *body position e* makes it difficult to design receiver of enough sensitivity at 10 MHz for the coupler dimensions of [1 × 1 ×

Table 2: Comparison of specific coupler/body positions in Figures 7(b) and 7(d) for higher propagation loss.

Coupler/body position 1	Coupler/body position 2	Comparison between positions 1 and 2 for higher propagation loss
Arm position a (102 cm)	—	Maximum propagation loss for arm positions in Figure 7(b)
Arm position f (135 cm)	Arm position a (102 cm)	Arm position a
Arm position d (53 cm)	Arm position e (53 cm)	Arm position d
Arm position c (116 cm)	Arm position b (116 cm)	Arm position b
Arm position c (116 cm)	Arm position d (53 cm)	Arm position d
Body position c (155 cm)	Body position a (83 cm)	Body position a
Body position c (155 cm)	Body position b (121 cm)	Body position b

0.5]. Therefore it can be inferred that minimum dimensions of the coupler are determined by different types of body wearables. The coupler dimensions dictate the receiver sensitivity and the communication distance.

4.3. Combined Effect of External Environment (Earth-Grounding, Material Structures). The effects on the propagation loss due to external furniture like wood, aluminium, or steel have been simulated in Figure 7(e) for scenarios in Figure 7(f). The horizontal ground-plane does not have the same effect on the propagation loss for different furniture materials which could be either conductors or insulators. The values of complex permittivity for these materials have been used from the built-in database provided by CST MWS, for example, the dispersive value of ϵ'' for wood varies exponentially between maximum 215 at 1 MHz and minimum 0.5 at 60 MHz, while ϵ' has a constant value of approximately 2.5 over the entire frequency range. Aluminium has superior conductive properties than both stainless steel and wood.

The aluminium table top in *Scenario c* provides a direct conductive path between transmitter and receiver couplers resulting in the lower propagation loss than *arm position e* in Figure 7(b) for the same distance of 53 cm. The radiated power starts becoming dominant for frequencies greater than 15 MHz which further lowers the propagation loss. The propagation loss for grounded aluminium table in *Scenario b* increases for frequencies up to 30 MHz compared to aluminium top in *Scenario b*. This effect could probably be explained by the additional signal loss due to the formation of closed loop through conductive aluminium table to ground-plane. But the radiated power which starts becoming dominant at higher frequencies compensates the effect of signal loss beyond 30 MHz for both *Scenario b* and *Scenario c*. The higher propagation loss could be observed in case of wooden table/top in *Scenario e* and *Scenario f* compared to aluminium table/top due to poor conductive properties of wood. The ground-plane has negligible effect on the propagation loss in case of closed loop formed by wooden table in *Scenario e* compared to wooden table top in *Scenario f*. The effect of greater radiated power in lowering propagation loss can be observed for higher frequencies. The external furniture could also result in asymmetrical propagation loss as shown for the grounded steel cupboard in *Scenario a* when the transmitter and receiver couplers change their positions from 1 to 2. The horizontal ground-plane and vertical grounded steel cupboard have lowering effect on the propagation loss when compared with *Arm Position a* in Figure 7(b). Air which is a poor conductor has maximum propagation loss for *Scenario d* shown in Figure 7(f) for the same distance of 53 cm. The simulated results in Figure 7(e) infer that the ground-plane has negligible effect on the propagation loss for insulators with dielectric properties like wood even when they make a closed loop between transmitting and receiving couplers with ground-plane. However for metallic conductors, for example, aluminium, the direct path between transmitting and receiving couplers compensate additional signal loss due to closed loop formed with the ground-plane. This signal loss is compensated by increased radiated power at higher frequencies.

4.4. Effect of Ground-Plane on the Resultant Electric Field. The electric field intensity plots are shown for a single cut along z-axis at 10 MHz frequency in Figure 8 so that the distribution of electric field in 2D along xy plane (area 305 × 261 cm^2) can be observed. There is a direct correlation between the propagation loss at 10 MHz in Figure 7(e) and the corresponding color mapping of E-field intensity plots in Figure 8. The electric field at the transmitter coupler is zero dB in these E-field plots.

The asymmetrical electric field distribution for *Scenario a* due to change in transmitting and receiving coupler positions is evident in electric field distribution plots. The conductive nature of aluminium provides a direct coupling path between transmitting and receiving couplers for *Scenario b* (aluminium table) compared to *Scenario e* (wooden table). The grounded aluminium table disturbs the electric field distribution below the table top more than the wooden table. The ground-plane under human model has almost no effect on the electric field distribution in *Scenario e* with wooden table compared to *Scenario e* without wooden table. This also shows that the ground-plane has negligible effect on the human body in terms of electric field distribution or propagation loss. The normalized electric field intensity for air medium at the receiver coupler is approximately −100 dB whereas it is −70 dB for *Scenario e* with human model in the absence of wooden table. This shows that human body is an energy efficient channel for signal transmission as compared to wireless transmission through air.

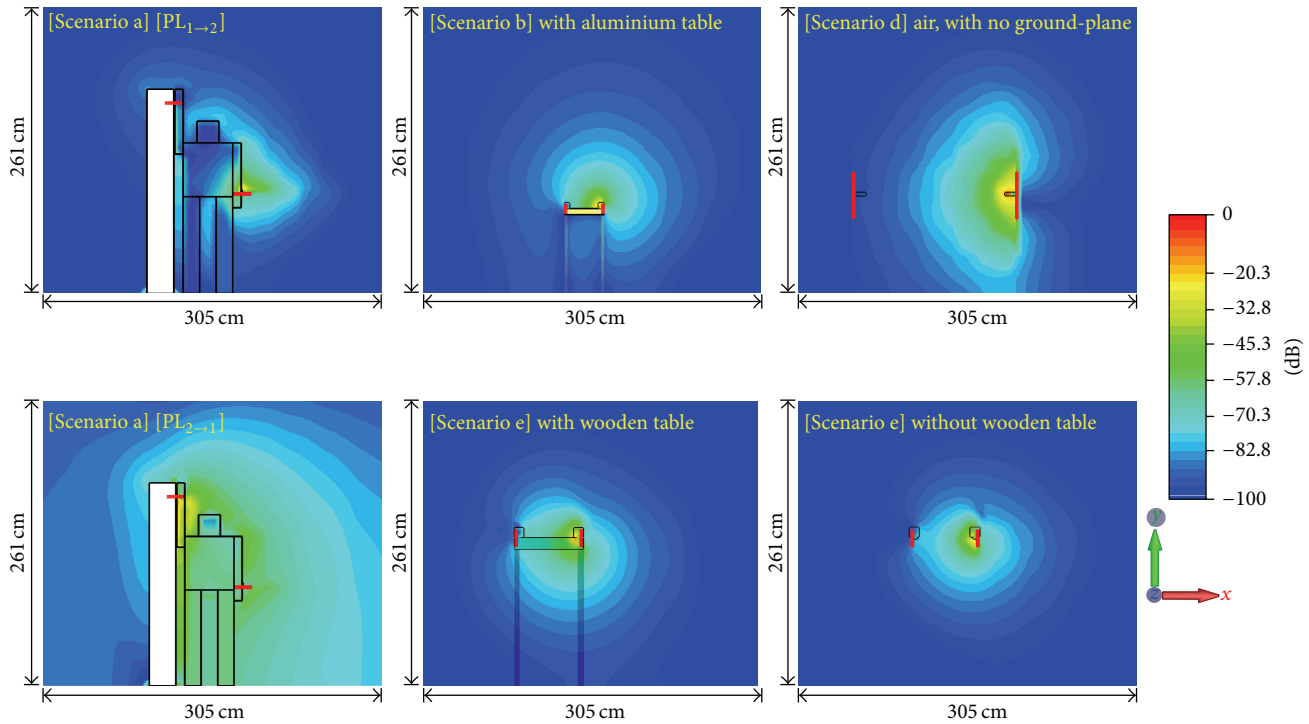

FIGURE 8: Electric field intensity plots showing distribution in xy plane (a single cut along z-axis) for selected scenarios in Figure 7(f).

4.5. Link-Budget Requirement for BCC. The motivation behind this close to real environment modeling and simulation is to find the link-budget requirement for designing capacitive BCC system in CMOS technologies. The design considerations include all possible scenarios, especially for the body wearable devices and estimated propagation losses which differ for a wide range of body positions, communication distances, coupler configuration, and sizes. The maximum available transmitted power P_{Tx} could be determined from foundry I/O pads which include features like electrostatic discharge (ESD) protection, essential for capacitive BCC scenarios when we are deliberately touching. As an example, the maximum current for analog I/O pads with ESD protection is 8 mA for 2.5 V supply for 65 nm CMOS technology which gives P_{Tx} of 13 dBm. The propagation loss of human body L_{HB} for *arm positions b to f* in Figure 7(b) is almost 80 dB at 10 MHz (Figure 7(a)) for the vertical coupler configuration with [4 × 4 × 1] dimensions. This coupler dimension is suitable for wrist watch as a body wearable device. So under perfect matching conditions on the transmitter (Tx) and receiver (Rx) side, the received power P_{Rx} at the reception coupler can be estimated as follows:

$$\begin{aligned} P_{\text{Rx}}\,(\text{dBm}) &= P_{\text{Tx}}\,(\text{dBm}) - L_{\text{HB}}\,(\text{dB}), \\ P_{\text{Rx}}\,(\text{dBm}) &= 13\,(\text{dBm}) - 80\,(\text{dB}) = -67\,(\text{dBm}). \end{aligned} \tag{3}$$

This means that the receiver should be sensitive enough to detect a minimum signal level of −67 dBm to cover the propagation loss due to *arm positions b to f* in Figure 7(b) at 10 MHz frequency.

5. Conclusion

A systematic efficient approach, based on simplified human modeling and full-wave EM simulation, has been proposed to realistically analyze the interaction of coupler, the human body (considering electrophysiological properties of tissues), and the environment all together for investigating the link-budget requirement for designing capacitive body-coupled communication system. The full-wave EM simulation strategy has been evaluated for numeric uncertainties (boundary conditions, mesh cells) and human body variation uncertainties (dielectric properties, dielectric thicknesses) independently for both vertical and horizontal couplers. After validating with the measurement results, the propagation loss for twenty different body positions in the mid-frequency range of 1 MHz to 60 MHz with communication distances up to 155 cm has been simulated. It is shown that the skin-only-rectangle human body model is accurate enough to predict the propagation loss for vertical couplers within 2 dB while the horizontal couplers have precision within 10 dB to 15 dB. Table 2 compares specific coupler/body positions which shows that the propagation loss characteristics are affected not only by the distance but also by the specific body positions and the propagation loss cannot be just scaled up for the longer communication distances based on the shorter distances. The comparison shows that the propagation loss in the arm-torso-arm region is the lowest when arms are not touching the torso region irrespective of the distance. The ground-plane has limited lowering effect on the propagation loss except when it has direct coupling with either transmitter or receiver coupler in the presence of metallic structures. The

coupler dimensions are determined by the requirement of body wearable device, which dictates the propagation loss. The link-budget has been investigated more realistically as a result of presented modeling and simulation approach.

Conflict of Interests

The authors declare that there is no conflict of interests regarding the publication of this paper.

References

[1] H. Baldus, S. Corroy, A. Fazzi, K. Klabunde, and T. Schenk, "Human-centric connectivity enabled by body-coupled communications," *IEEE Communications Magazine*, vol. 47, no. 6, pp. 172–178, 2009.

[2] S.-J. Song, N. Cho, S. Kim, J. Yoo, and H.-J. Yoo, "A 2Mb/s wideband pulse transceiver with direct-coupled interface for human body communications," in *Proceedings of the IEEE International Solid-State Circuits Conference (ISSCC '06)*, pp. 2278–2287, IEEE, San Francisco, Calif, USA, February 2006.

[3] A. Fazzi, S. Ouzounov, and J. van den Homberg, "A 2.75 mW wideband correlation-based transceiver for body-coupled communication," in *Proceedings of the IEEE International Solid-State Circuits Conference—Digest of Technical Papers (ISSCC '09)*, pp. 204–205, San Francisco, Calif, USA, February 2009.

[4] T. G. Zimmerman, "Personal area networks: Near-field intrabody communication," *IBM Systems Journal*, vol. 35, no. 3-4, pp. 609–617, 1996.

[5] N. Cho, J. Yoo, S.-J. Song, J. Lee, S. Jeon, and H.-J. Yoo, "The human body characteristics as a signal transmission medium for intrabody communication," *IEEE Transactions on Microwave Theory and Techniques*, vol. 55, no. 5, pp. 1080–1085, 2007.

[6] J. Bae, H. Cho, K. Song, H. Lee, and H.-J. Yoo, "The signal transmission mechanism on the surface of human body for body channel communication," *IEEE Transactions on Microwave Theory and Techniques*, vol. 60, no. 3, pp. 582–593, 2012.

[7] K. Hachisuka, Y. Terauchi, Y. Kishi et al., "Simplified circuit modeling and fabrication of intrabody communication devices," *Sensors and Actuators, A: Physical*, vol. 130-131, pp. 322–330, 2006.

[8] N. Haga, K. Saito, M. Takahashi, and K. Ito, "Proper derivation of equivalent-circuit expressions of intra-body communication channels using quasi-static field," *IEICE Transactions on Communications*, vol. E-95-B, no. 1, pp. 51–59, 2012.

[9] N. Haga, K. Saito, M. Takahashi, and K. Ito, "Equivalent circuit of intrabody communication channels inducing conduction currents inside the human body," *IEEE Transactions on Antennas and Propagation*, vol. 61, no. 5, pp. 2807–2816, 2013.

[10] M. S. Wegmueller, A. Kuhn, J. Froehlich et al., "An attempt to model the human body as a communication channel," *IEEE Transactions on Biomedical Engineering*, vol. 54, no. 10, pp. 1851–1857, 2007.

[11] K. Fujii and Y. Okumura, "Effect of earth ground and environment on body-centric communications in the MHz band," *International Journal of Antennas and Propagation*, vol. 2012, Article ID 243191, 10 pages, 2012.

[12] K. Norton, "The propagation of radio waves over the surface of the earth and in the upper atmosphere," *Proceedings of the IRE*, vol. 24, no. 10, pp. 1367–1387, 1936.

[13] K. Norton, "The propagation of radio waves over the surface of the earth and in the upper atmosphere," *Proceedings of the Institute of Radio Engineers*, vol. 25, no. 9, pp. 1203–1236, 1937.

[14] S. Gabriel, R. W. Lau, and C. Gabriel, "The dielectric properties of biological tissues: III. Parametric models for the dielectric spectrum of tissues," *Physics in Medicine and Biology*, vol. 41, no. 11, pp. 2271–2293, 1996.

[15] IFAC-CNR, *An Internet Resource for the Calculation of the Dielectric Properties of Body Tissues in the Frequency Range 10 Hz–100 GHz*, IFAC-CNR, Florence, Italy, 1997, http://niremf.ifac.cnr.it/tissprop/.

[16] T. C. W. Schenk, N. S. Mazloum, L. Tan, and P. Rutten, "Experimental characterization of the body-coupled communications channel," in *Proceedings of the IEEE International Symposium on Wireless Communication Systems (ISWCS '08)*, pp. 234–239, October 2008.

[17] N. S. Mazloum, *Body-coupled communications: experimental characterization, channel modeling and physical layer design [M.S. thesis]*, Department of Signals and Systems Distributed Sensor Systems, Chalmers University of Technology Philips Research, Gothenburg, Sweden, 2008.

[18] Computer Simulation Technology (CST), 2015, http://www.cst.com/.

[19] M. Clemens and T. Weiland, "Discrete electromagnetism with the finite integration technique," *Progress in Electromagnetics Research*, vol. 32, pp. 65–87, 2001.

[20] Y. Song, K. Zhang, Q. Hao, L. Hu, J. Wang, and F. Shang, "A finite-element simulation of galvanic coupling intra-body communication based on the whole human body," *Sensors*, vol. 12, no. 10, pp. 13567–13582, 2012.

[21] J. A. Ruiz and S. Shimamoto, "Experimental evaluation of body channel response and digital modulation schemes for intrabody communications," in *Proceedings of the IEEE International Conference on Communications (ICC '06)*, vol. 1, pp. 349–354, IEEE, Istanbul, Turkey, June 2006.

[22] R. Xu, H. Zhu, and J. Yuan, "Electric-field intrabody communication channel modeling with finite-element method," *IEEE Transactions on Biomedical Engineering*, vol. 58, no. 3, pp. 705–712, 2011.

[23] J. Sakai, L.-S. Wu, H.-C. Sun, and Y.-X. Guo, "Balun's effect on the measurement of transmission characteristics for intrabody communication channel," in *Proceedings of the IEEE MTT-S International Microwave Workshop Series on RF and Wireless Technologies for Biomedical and Healthcare Applications (IMWS-BIO '13)*, pp. 1–3, December 2013.

[24] R. Xu, H. Zhu, and J. Yuan, "Circuit-coupled FEM analysis of the electric-field type intra-body communication channel," in *Proceedings of the IEEE Biomedical Circuits and Systems Conference (BioCAS '09)*, pp. 221–224, November 2009.

[25] H. Zhu, R. Xu, and J. Yuan, "High speed intra-body communication for personal health care," in *Proceedings of the Annual International Conference of the IEEE Engineering in Medicine and Biology Society (EMBC '09)*, pp. 709–712, IEEE, Minneapolis, Minn, USA, September 2009.

[26] K. Fujii, M. Takahashi, and K. Ito, "Electric field distributions of wearable devices using the human body as a transmission channel," *IEEE Transactions on Antennas and Propagation*, vol. 55, no. 7, pp. 2080–2087, 2007.

[27] M. S. Wegmueller, S. Huclova, J. Froehlich et al., "Galvanic coupling enabling wireless implant communications," *IEEE*

Transactions on Instrumentation and Measurement, vol. 58, no. 8, pp. 2618–2625, 2009.

[28] M. S. Wegmüller, *Intra-body communication for biomedical sensor networks [Ph.D. thesis]*, Eidgenössische Technische Hochschule ETH, Zürich, Switzerland, 2007.